Photochemistry and Photobiology, 2006, 82: 1226–1232

Symposium-in-Print: Singlet Oxygen

A Comparison of Intrazeolite and Solution Singlet Oxygen Ene Reactions of Allylic Alcohols

Edward L. Clennan*, Dong Zhang and Jamie Singleton

Department of Chemistry, University of Wyoming, 1000 East University Avenue, Laramie, WY

Received 09 January 2006; accepted 23 January 2006; published online 31 January 2006 DOI: 10.1562/2006-01-09-RA-768

ABSTRACT

The singlet oxygen ene reactions of four allylic alcohols and for comparison an allylic ether have been examined both in solution and in zeolite Y. Brønsted acid sites in the zeolite were shown to induce decomposition of several of the allylic alcohols. Treatment of the zeolites with pyridine removed these acid sites and allowed intrazeolite reactions of the allylic alcohols without interference from decomposition. Control reactions with an allylic alcohol that is inert to decomposition provided evidence that the presence of pyridine in the zeolite labyrinth does not influence the product composition.

INTRODUCTION

The use of molecular oxygen as a terminal oxidant is attractive from both economic and environmental perspectives. Consequently, the singlet oxygen ene reaction (Eq. 1) has attracted considerable attention since it was first reported by G. O. Schenck more than 50 years ago (1). The well-established stereochemical features of this reaction provide predictive power that adds to its synthetic utility (2). For example, it is a suprafacial process with oxygen and hydrogen removal occurring from the same face of the alkene (3,4). In addition; (1) only those hydrogen that are, or can be, aligned perpendicular to the π-system are subject to removal; (2) hydrogens that are on the more highly crowded side of the alkene are preferentially abstracted (*cis* effect); and (3) hydrogen bonding, steric, and electronic interactions with the trailing pendant oxygen in the perepoxide (Eq. 1) can be used to direct the regiochemistry of hydrogen removal (5). Nevertheless, in many substrates multiple hydrogens can meet these stereoelectronic requirements for abstraction and product mixtures are often observed.

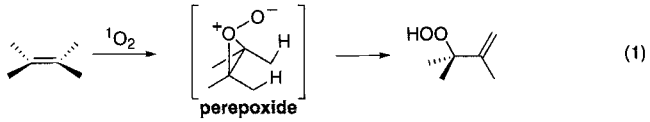

(1)

*Corresponding author email: clennane@uwyo.edu (Edward L. Clennan)

Photo-oxygenations in heterogeneous media have become increasingly popular as a means to improve or reverse the substrate-induced regiochemistry of the singlet oxygen ene reaction. In this report we describe our recent efforts to use zeolites to influence the singlet oxygen ene reactions of a series of allylic alcohols. For this work we have chosen to use zeolite Y (NaY; Fig. 1) because of its availability and suitable pore and cavity size that can readily accommodate the organic substrates. NaY is an aluminosilicate honeycomb network with $[SiO_4]^{4-}$ and $[AlO_4]^{5-}$ vertices that form 13-Å-diameter supercages that are interconnected via tetrahedrally arranged 7.4-Å pores (6,7). The cations (*e.g.* Na^+) found in the interior of the zeolite are necessary to balance the negative charge on the tetravalent aluminum atoms and create a highly charged electrostatic and unique reaction environment. Li and Ramamurthy took advantage of these exchangeable cations in 1996 to introduce thiazine into the zeolite and to conduct the first intrazeolite singlet oxygen reactions (8).

MATERIALS AND METHODS

The allylic alcohol substrates 3-methyl-2-buten-1-ol and 3-methyl-2-cyclohexen-1-ol were purchased from Aldrich and used without further purification. The substrates 4-methyl-3-penten-2-ol (9), E-3-methyl-3-penten-2-ol (9), and Z-4-methoxy-2-methyl-2-pentene (9) were synthesized using literature procedures. NaY (lot number JI20903EI) was purchased from Aldrich and prepared for reaction as described below. All reaction mixtures were monitored by proton NMR on a Bruker DRX-400 and product ratios determined by careful integration.

Solution photo-oxidations. All solution photo-oxidations were conducted using $CDCl_3$ reaction mixtures, 0.2 M in substrate and 1×10^{-4} M in tetraphenylporphyrin. Each reaction mixture was saturated with dry oxygen for 10 min before irradiation and bubbling was continued during irradiation. The bubbling rate was controlled to prevent loss of the solvent and the irradiations were conducted with a 600-W tungsten–halogen lamp through 1 cm of a 12 M (saturated) $NaNO_2$ solution ($\lambda_{irradiation} > 400$ nm). All reaction mixtures were analyzed immediately by NMR and in some cases both before and after reduction of the allylic hydroperoxide products with triphenylphosphine.

Preparation of methylene blue exchange zeolite Y. NaY was stirred for 24 h in a 1 M aqueous NaCl solution, filtered and washed with deionized distilled water. This procedure was repeated for a total of three times and the NaY dried at 120°C in a vacuum oven for 24 h. This treatment ensured the elimination of other cations and the removal of the majority of the Brønsted acid sites in the supercages. Enough methylene blue (25.2 mg) to provide a loading level of one molecule per 100 supercages ($\langle S \rangle = 0.01$) was added to 350 mL of aqueous slurry of 14.6 g of NaY and stirred for 48 h in the dark. The slurry was then centrifuged and the transparent aqueous solution decanted. The colored residue was then washed five times with 50 mL of water. During this process no dye was extracted from the

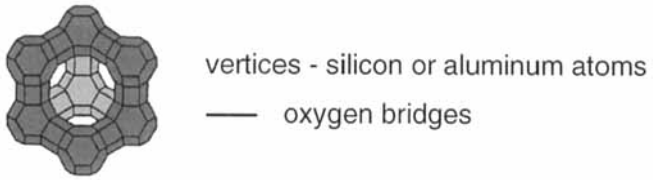

Figure 1. A depiction of NaY showing the 7.4-Å windows leading into the 13-Å diameter supercage.

zeolite into the aqueous layer. The MB@NaY($\langle S \rangle = 0.01$) was covered with aluminum foil and air dried in the dark for 2 days and then dried on a vacuum line at 95°C and 10^{-4} torr for 3 days before use.

Zeolite photo-oxygenations. A small amount of pyridine (approximately 1 mg) was added to 5 mL of freshly distilled hexane. To this solution 0.3 g of dry MB@NaY($\langle S \rangle = 0.01$) was added to generate a pyridine-supplemented zeolite ($\langle S \rangle_{pyridine} = 0.06$ to 0.1). The hexane slurry was then saturated with oxygen and enough substrate added to give a loading level of $\langle S \rangle_{substrate} = 0.5$. The reaction mixture was then immediately irradiated under continuous oxygen agitation with a 600-W tungsten–halogen lamp for about 10 min through 1 cm of a 12 M (saturated) $NaNO_2$ solution ($\lambda_{irradiation} > 400$ nm). After photolysis the reaction mixture was centrifuged and the hexane removed. The products were immediately extracted with freshly distilled tetrahydrofuran (THF). The THF was then removed with care with a rotary evaporator and the residue immediately analyzed by ^1H NMR. The mass balances were determined by integration relative to an internal standard.

Photo-oxygenation of allylic alcohol 1. **3-methyl-2-buten-1-ol (1).** ^1H NMR ($CDCl_3$) δ 1.26 (bs, 1H), 1.71 (s, 3H), 1.77 (s, 3H), 4.16 (d, J = 7 Hz, 2H), 5.44 (t, J = 7 Hz, 1H). **3-methyl-2-butenal (2).** ^1H NMR ($CDCl_3$) δ 2.01 (s, 3H), 2.17 (s, 3H), 5.93 (d, J = 8 Hz, 1H), 9.99 (d, J = 8 Hz, 1H). **3,3-dimethyl-oxirane-2-carbaldehyde (3).** ^1H NMR ($CDCl_3$) δ 1.46 (s, 3H), 1.50 (s, 3H), 3.21 (d, J = 5 Hz, 1H), 9.48 (d, J = 5 Hz, 1H). **2-hydroperoxy-3-methyl-3-buten-1-ol (4).** ^1H NMR ($CDCl_3$) δ 1.82 (s, 3H), 3.77 (d, J = 5.6 Hz, 2H), 4.56 (t, J = 5.6 Hz, 1H), 5.12 (bs, 2H). The allylic hydroperoxide was reduced with PPh_3 to give **3-methyl-3-buten-1,2-diol** ^1H NMR ($CDCl_3$) δ 1.77 (s, 3H), 3.58 (dd, J = 7.3, 11.2 Hz, 1H), 3.72 (dd, J = 3.4, 11.2 Hz, 1H), 4.20 (dd, J = 3.4, 7.3 Hz, 1H), 4.97 (s, 1H), 5.09 (s, 1H). The 1,2-dioxolane, **5**, was not reduced even after standing in the presence of PPh_3 for 2 weeks. **5,5-dimethyl-[1,2]dioxolan-3-ol (5).** ^1H NMR ($CDCl_3$) δ 1.37 (s, 3H), 1.46 (s, 3H), 2.38 (dd, J = 1.6, 13 Hz, 1H), 2.71 (dd, J = 5.9, 13 Hz, 1H), 5.70 (dd, J ~ 1, 5.7 Hz, 1H). **Hemiacetals (3′ and 3″)** ^1H NMR (CD_3OD) δ 1.29 (s, 3H), 1.30 (s, 3H), 1.31 (s, 3H), 1.33 (s, 3H), 2.73 (d, J = 6.5 Hz, 1H), 2.75 (d, J = 7.0Hz, 1H), 4.28 (d, J = 7.0Hz, 1H), 4.31 (d, J = 6.5 Hz, 1H). ^{13}C NMR (CD_3OD) δ 19.38, 19.49, 24.91, 24.96, 59.41, 59.80, 66.13, 66.40, 98.52, 98.05, CD_3 groups obscured by CD_3OD.

Photo-oxygenation of allylic alcohol 6. **4-methyl-3-buten-2-ol (6).** ^1H NMR ($CDCl_3$) δ 1.26 (d, J = 6 Hz, 3H), 1.32–1.35 (bs, 1H), 1.72 (d, J = 1.3 Hz, 3H), 1.74 (d, J = 1.4 Hz, 3H), 4.55–4.65 (m, 1H), 5.23–5.28 (m, 1H). **S*S*-3-hydroperoxy-4-methyl-4-penten-2-ol (7).** ^1H NMR ($CDCl_3$) δ 1.09 (d, J = 6.4 Hz, 3H), 1.70 (dd, J = 1.3, 1.0 Hz, 3H), 3.63 (bs, 1H), 3.84 (dq, 8.6, 6.4 Hz, 1H), 4.12 (d, J = 8.6 Hz, 1H), 5.08–5.10 (m, 2H), 9.44 (bs, 1H). **S*R*-3-hydroperoxy-4-methyl-4-penten-2-ol (8).** ^1H NMR ($CDCl_3$) δ 1.18 (d, J = 6.4 Hz, 3H), 1.78 (dd, J = 1.2, 1.0 Hz, 3H), 2.54 (bs, 1H), 3.95 (dq, J = 6.4, 4.9 Hz, 1H), 4.28 (d, J = 4.9 Hz, 1H), 5.04–5.06 (m, 2H), 9.17 (bs, 1H). **3, 5, 5-trimethyl-[1,2]dioxolan-3-ol (9).** An AB quartet similar to that reported (9) reveals a trace of **9**; however, the singlets associated with the methyl groups could not be assigned with certainty. ^1H NMR ($CDCl_3$) δ 2.41 (d, J = 12.8 Hz), 2.50 (d, J = 12.8 Hz).

Photo-oxygenation of allylic alcohol 10. **E-3-methyl-3-penten-2-ol (10).** (9) ^1H NMR ($CDCl_3$) δ 1.25 (d, J = 8.0 Hz, 3H), 1.60 (d, J = 6.7 Hz, 3H)*, 1.63 (s, 3H)*, 4.21 (q, J = 6.4 Hz, 1H), 5.49 (dqq, J = 1.1, 1.1, 6.6 Hz, 1H) *some unresolved long-range coupling. **S*S*-3-hydroperoxy-3-methyl-4-penten-2-ol (11).** ^1H NMR ($CDCl_3$) δ 1.14 (d, J = 6.5 Hz, 3H), 1.28 (s, 3H), 4.02 (q, J = 6.5 Hz, 1H), region between 5.32 and 5.4 severe overlap between **11** and **12**, 5.92 (dd, J = 11, 17.7 Hz, 1H), 8.27 (bs, 1H). **S*R*-3-hydroperoxy-3-methyl-4-penten-2-ol (12).** ^1H NMR ($CDCl_3$) δ 1.14 (d, J = 6.6 Hz, 3H), 1.34 (s, 3H), 3.99 (q, J = 6.6 Hz, 1H), region between 5.32 and 5.4 severe overlap between **11** and **12**, 5.99 (dd, J = 11.2, 17.7 Hz, 1H), 8.35 (bs, 1H). **S*R*-4-hydroperoxy-3-methylene-2-pentanol (13).** ^1H NMR ($CDCl_3$) δ 1.30 (d, J = 7.3 Hz, 3H), 1.39 (d, J = 6.5 Hz, 3H), 4.49 (dq, J = 0.8, 6.5 Hz, 1H), 4.71 (q, J = 6.6 Hz, 1H), 5.21 (m, 1H), 5.32 (m, 1H), 9.61 (bs, 1H). **S*S*-4-hydroperoxy-3-methylene-2-pentanol (14).** ^1H NMR ($CDCl_3$) δ 1.38 (d, J = 6.6 Hz, 3H), 1.40 (d, J = 6.5 Hz, 3H), 4.44 (dq, J = 0.9, 6.5 Hz, 1H), 4.64 (dq, J = 0.9, 6.6 Hz, 1H), 5.21 (m, 1H), 5.32 (m, 1H), 9.01 (bs, 1H).

Photo-oxygenation of allylic alcohol 15. **3-methyl-2-cyclohexenol (15)** ^1H NMR ($CDCl_3$) δ 1.3-2.0 (m, 7H), 1.69 (s, 3H), 4.18 (bs, 1H), 5.50 (bs, 1H). ^{13}C NMR ($CDCl_3$) δ 19.19, 23.77, 30.20, 31.79, 65.95, 124.48, 138.68. **3-methyl-2-cyclohexenone (20)** ^1H NMR ($CDCl_3$) δ 1.96 (s, 3H), 1.99 (pent, J = 8Hz, 2H), 2.28 (t, J = 8Hz, 2H), 2.34 (t, J = 8Hz, 2H), 5,88 (bs, 1H). ^{13}C NMR ($CDCl_3$) δ 22.61, 24.52, 30.99, 37.05, 126.69, 162.93, 199.81. The allylic hydroperoxides were identified by reduction with triphenylphosphine to the diols followed by comparison to published proton and carbon NMR of these compounds. ***cis*-3-methylene-1,2-cyclohexandiol (16-OH)**, (10) ***trans*-3-methylene-1,2-cyclohexandiol (16-OH)** (10), ***cis*-3-methyl-3-cyclohexen-1,2-diol (18-OH)** (11), **3-methyl-2,3-epoxy-cyclohexanone (21)** (12). Spectral data for the *trans*-1,2-diol, ***trans*-3-methyl-3-cyclohexen-1,2-diol (19-OH)** is not available but it is tentatively assigned on the basis of comparison of ^{13}C NMR chemical shifts in the reaction mixture and comparison with those published for **18-OH** (11). ***trans*-3-methyl-3-cyclohexen-1,2-diol (19-OH)** ^{13}C NMR ($CDCl_3$) tentative δ 19.63, 22.35, 73.88, 76.10, 123.75, quaternary vinyl carbon not observed.

Photo-oxygenation of allylic ether 22. **4-methoxy-2-methyl-2-pentene (22)** ^1H NMR ($CDCl_3$) δ 1.17 (d, J = 8Hz, 3H), 1.67 (d, J = 1.4Hz, 3H), 1.74 (d, J = 1.4Hz, 3H), 4.03 (dq, J = 9, 6 Hz, 1H), 5.55 (d with further small coupling, J = 9Hz, 1H). **(S*S*)-4-methoxy-2-methyl-1-penten-3-yl hydroperoxide (23)** ^1H NMR ($CDCl_3$) δ 1.10 (d, J = 6Hz, 3H), 1.76 (dd, J = 1.2, 1.5 Hz, 3H), 3.44 (s, 3H), 3.54 (dq, J = 8.2, 6.4 Hz, 1H), 4.28 (d, J = 8.2Hz, 1H), no vinyl hydrogens obscured by starting material, 9.35 (s, 1H). **(S*R*)-4-methoxy-2-methyl-1-penten-3-yl hydroperoxide (24)** ^1H NMR ($CDCl_3$) δ 1.16 (d, J = upfield peak obscured by starting material), 1.80 (m, 3H), 3.38 (s, 3H), ≈ 3.55 (peaks obscured by S*S* isomer), 4.41 (d, J = 4.4Hz, 1H), 5.08–5.10 (m, 2H), 8.70 (s, 1H).

RESULTS

Solution studies

Allylic alcohols **1**, **6**, **10**, **15**, and for comparison, allylic ether **22**, react with singlet oxygen in $CDCl_3$ to give the products shown in Chart 1.

3-Methyl-2-buten-1-ol, **1** (13), reacts by hydrogen abstraction predominately at the gem–dimethyl end of the alkene to give allylic hydroperoxide, **4**. Without labeling it is impossible to determine the extent of reaction at each of the diastereomeric methyls; however, given the preference for the stereoelectronic "cis-effect," hydrogen abstraction likely prevails from the Z-methyl group. Hydrogen abstraction from the carbinol carbon, however, is significant and can account for the formations of **2**, **3** and **5**, as shown in Fig. 2. Although formation of **3** could be attributed to reaction of **2** with adventitious hydrogen peroxide, this reaction normally requires basic conditions (14). In addition, there does not appear to be an induction period for the formation of **3**. Consequently, we suggest that it is a primary oxidation product formed by intramolecular displacement of hydroxide (or water) in the enolic–allylic–hydroperoxide intermediate, **II** (Fig. 2).

In methanol the reaction of **1** with singlet oxygen was significantly altered from that observed in $CDCl_3$. The allylic hydroperoxide was reduced from 70% of the reaction mixture in $CDCl_3$ to only 47% of the reaction mixture in CD_3OD. In addition, two novel diastereomeric hemiacetals, **3′** and **3″** (Fig. 2), formed, presumably by the addition of methanol to protonated **3**. We suggest that intermolecular hydrogen bonding of the hydroxyl group in perepoxide I (Fig. 2) with methanol competes with the intramolecular hydrogen bond (bond **a** in structure **I** in Fig. 2) to the pendant oxygen. In the absence of this intramolecular hydrogen bond (bond **a**, Fig. 2) the allylic hydroxyl group is free to rotate to

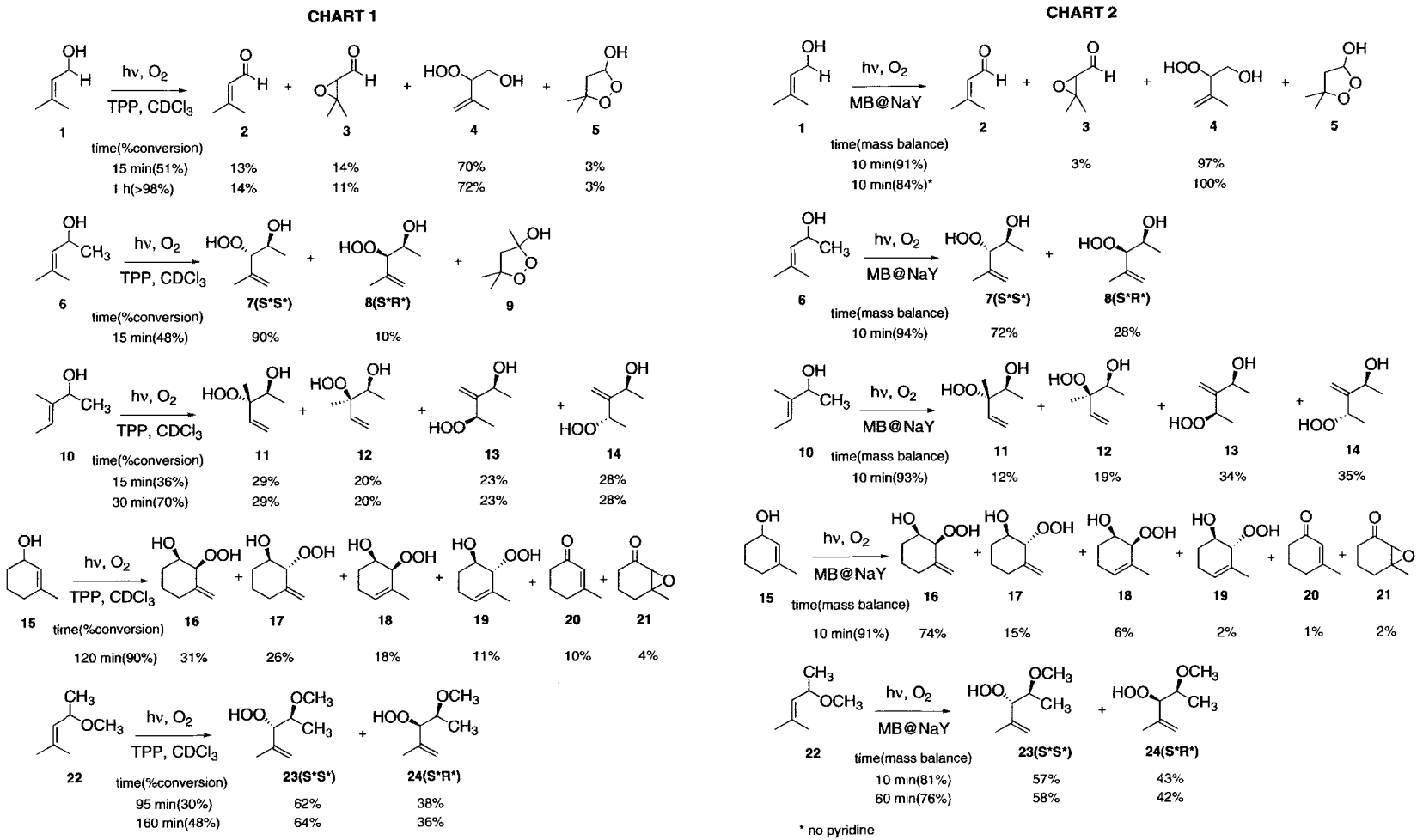

Chart 1. A comparison of products in solution and in NaY singlet oxygen ene reactions.

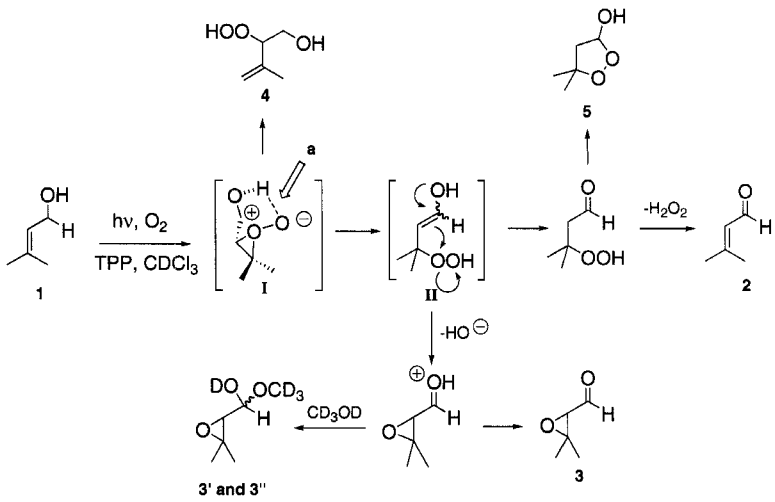

Figure 2. Mechanism for reaction of allylic alcohol **1** with singlet oxygen.

place the allylic hydrogens (-CH_2-OH) in the perpendicular geometry necessary for abstraction to form an increased amount of allylic hydroperoxide II and ultimately **3′** and **3″** (Fig. 2).

Allylic alcohol, 4-methyl-3-buten-2-ol, **6**, was a key substrate in the elegant work of Adam and coworkers (9,15–20) that was used to establish the importance of hydrogen bonding as a directing element in singlet oxygen ene reactions. Three rotomers of the S enantiomer of **6** are shown in Fig. 3. Attack from the bottom face of each rotomer leads to the major S*S* (threo) product, whereas attack from the top face leads to the minor S*R* (erythro) product. If the cis effect were dictating the observed stereochemistry the preferred perepoxide transition structure would be either **A** or **E**, both of which have the greatest number of interactions between cis-allylic hydrogens and the trailing oxygen in the perepoxide. However, if this were the case the S*R* product would predominate, contrary to what is observed since the $A_{1,3}$ strain between the H- and Me- groups in **E** is more destabilizing than the $A_{1,3}$ strain between the H- and HO- groups in **A**. Consequently, Adam and coworkers suggested that hydrogen bonding to the pendant oxygen in the perepoxide transition structure dictated product regiochemistry. As a result, hydrogen-bonded transition structure **D**, with less $A_{1,3}$ strain than hydrogen-bonded transition structure **C** with the greater H-/Me- $A_{1,3}$ strain, preferentially leads to the S*S* (threo) product by a factor of 9:1.

The importance of hydrogen bonding as a directing element is verified by the reactivity of 4-methoxy-2-methyl-2-butene, **22**, in which the possibility of hydrogen bonding has been eliminated by replacement of the HO- group with the CH_3O- group (9). In this case the threo (S*S*) product is still preferred but by less than a factor of 2:1.

The steering effect of the hydroxyl group must be coupled with a conformational bias for a single conformation. This bias is absent in **10** because of the lack of a cis-methyl group and the concomitant allylic ($A_{1,3}$) strain. As a result, photo-oxygenation of **10** shows complete loss of diastereoselectivity and little regiochemical preference. The hydroxyl group in cycloalkene **15** also exhibits little if any steering effect. Force field calculations reveal that **15** exists in a half-chair conformation with only a slight preference

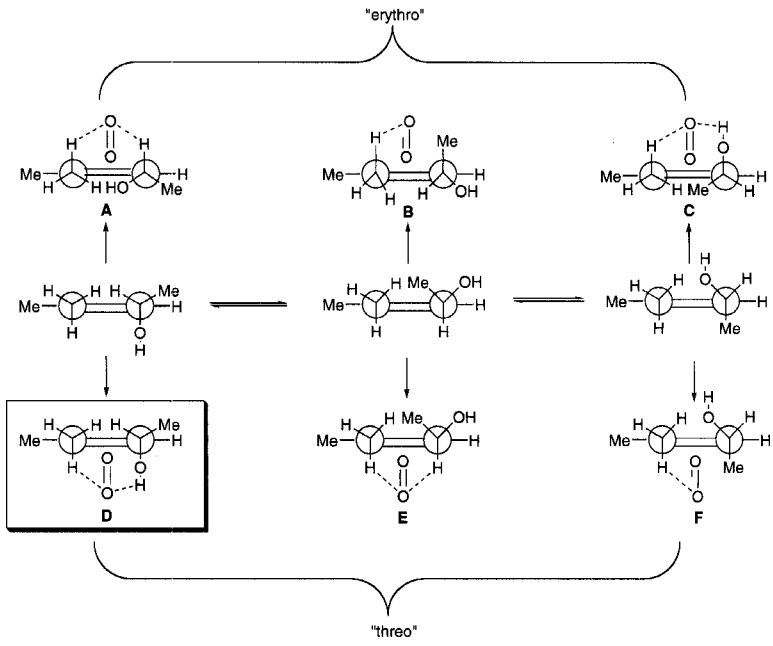

Figure 3. Reactions of three rotomers of the S enantiomer of allylic alcohol **6** on the erythrotopic and threotopic faces.

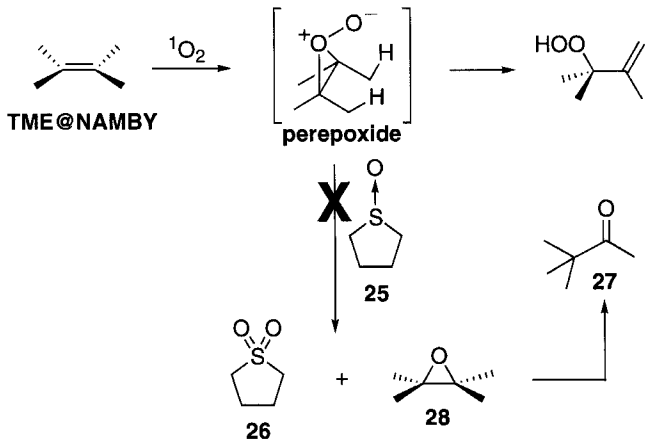

Figure 4. Attempted intrazeolite trapping of a perepoxide intermediate.

for the equatorial ($\Delta H_f = -51.19$ kcal mol^{-1}) rather than the axial ($\Delta H_f = -50.95$ kcal mol^{-1}) hydroxyl group.

Zeolite studies. Allylic alcohols **1**, **6**, **10**, **15**, and for comparison, allylic ether, **22**, react with singlet oxygen in hexane slurries in the presence of pyridine-supplemented MB@NaY to give the products shown in Chart 1. Gas chromatography (GC) analysis of the hexane demonstrated that all the starting materials migrated quantitatively into the zeolite before irradiation. The pyridine at levels between 0.6 and 1.0 molecules per supercage (*i.e.* $\langle s \rangle = 0.6$ to 1.0) was necessary to prevent acid-catalyzed rearrangements of the allylic alcohols. Allylic alcohol **1** was the exception. It could be successfully extracted from the zeolite after an extended residence time (≈2 h) without visible decomposition. We attribute this stability to the fact that **1** forms a less-stable 1,1-disubstituted allylic cation, whereas **6**, **10** and **15** form more-stable 1,1,3-trisubstituted allylic cations. The stability of **1** in the zeolitic environment allowed us to show that the product composition is essentially unchanged in pyridine-supplemented and -unsupplemented photo-oxygenations. (Chart 1) The inability to isolate from the zeolite the small amount of epoxide, **3**, formed in the reaction of **1** in the absence of pyridine was expected. We have previously shown that epoxides formed during photo-oxygenations of 1,1-diarylethylenes are susceptible to acid-catalyzed rearrangements and could only be isolated from zeolite samples pretreated with pyridine (21).

We have also conducted intrazeolite cophoto-oxidations with thiolane sulfoxide, **25** (Fig. 4), in an attempt to trap a perepoxide intermediate. These studies were done using the reactive singlet oxygen substrate 2,3-dimethyl-2-butene in MB@NaY($\langle S \rangle = 0.01$). The trapping studies were conducted with loading levels of $\langle S \rangle_{TME} = 0.50$, and $\langle S \rangle_{25} = 0.80$ and 1.0. The photo-oxygenations were conducted as described in the Materials and Methods section and the products analyzed by GC after reduction with triphenylphosphine. In no case was thiolane sulfone, **26**, pinacolone, **27**, or tetramethyl oxirane, **28**, observed by GC using authentic independently synthesized samples.

DISCUSSION

A comparison of the product compositions in solution with those formed in the zeolite (Chart 1) demonstrate that there are medium effects on both the regio- and stereochemistry of the singlet oxygen ene reactions of allylic alcohols. The regiochemical changes are especially evident in the photo-oxygenations of **1**, **10** and **15**. In each of these cases hydrogen abstraction from the most highly substituted end of the alkene is enhanced upon moving the reaction from solution into the zeolite. The ratio of hydrogen abstraction from the most highly substituted to the less substituted end of the alkene changes from 2.33 {[**4**]/([**2**] + [**3**] + [**5**])} for **1**, from 1.04 {([**13**] + [**14**])/([**11**] + [**12**])} for **10** and from 6.14 {([**16**] + [**17**] + [**18**] + [**19**])/([**20**] + [**21**])} for **15** in solution to 32.33, 2.22 and 32.33, respectively, in the zeolitic medium (21). In addition, the side selectivity, ([**16**] + [**17**])/([**18**] + [**19**]), for **15** dramatically changes from 1.97 in solution to 11.12 in the interior of the zeolite.

These regiochemical changes are reminiscent of those observed during intrazeolite photo-oxygenations of trisubstituted alkenes as shown in Fig. 5 (22). In these cases hydrogen abstraction from the disubstituted end of the alkene increases dramatically when the reaction is moved from solution into the zeolite. In addition, most of this increase is due to increased hydrogen abstraction from the least substituted side of the alkene.

To rationalize these results we have suggested the model shown in Fig. 6 (3). The key feature of this model involves complexation of the alkene to a sodium cation within the zeolite supercage. Alkali metal cation complexation to alkenes is well documented both in solution and in the gas phase (23,24). This complexation occurs on the least-hindered face of the alkene and forces singlet oxygen to approach from the most-hindered face. As the oxygen

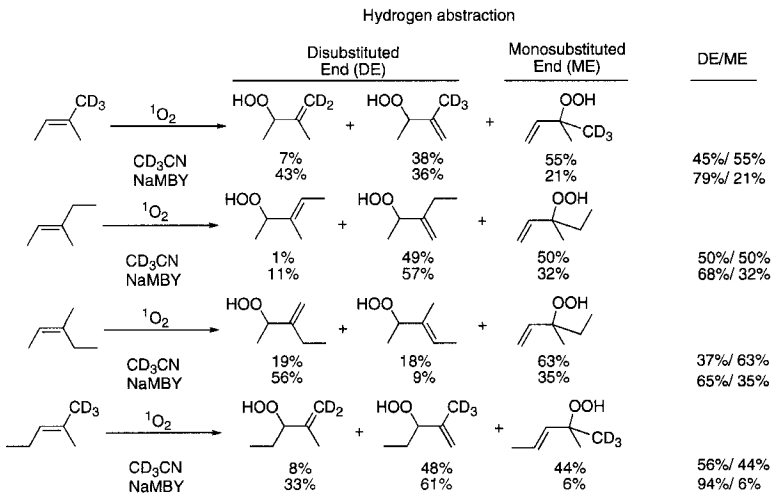

Figure 5. A regiochemical comparison of solution and intrazeolite singlet oxygen ene reactions of trisubstituted alkenes.

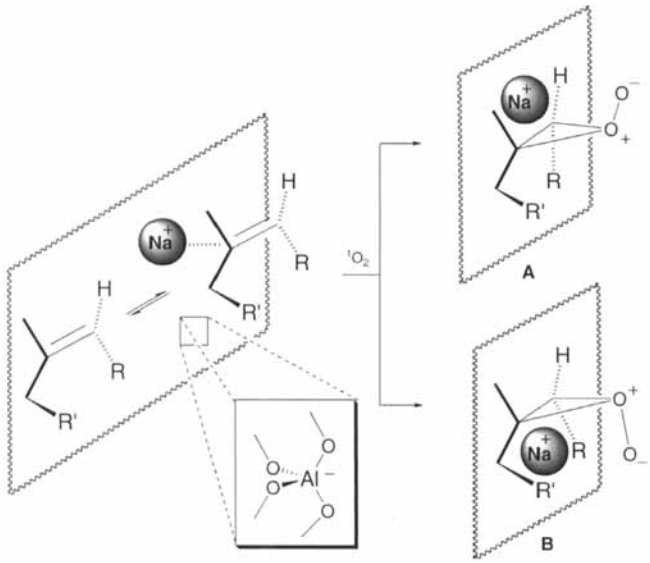

Figure 6. A model for intrazeolite singlet oxygen ene reactions of allylic alcohols.

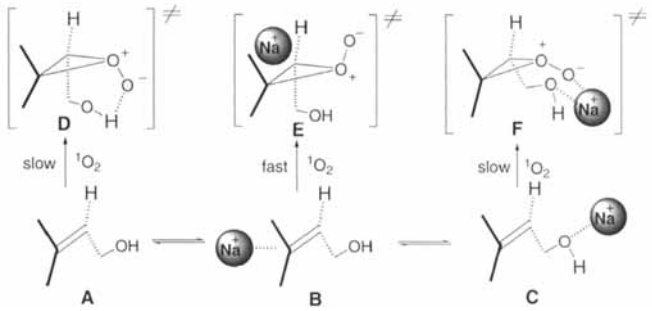

Figure 7. A Curtin–Hammett analysis of intrazeolite transition state cation binding geometries of allylic alcohols.

approaches the sodium cation moves to provide electrostatic stabilization to the nascent perepoxide. This stabilization leads to a remarkable intrazeolite rate enhancement in comparison to solution (see Chart 1). For example, allylic ether **22** requires 95 min in solution for a 30% conversion to product, whereas in the zeolite 81% conversion is realized in only 10 min of irradiation. However, these are qualitative and not quantitative results. Nevertheless, these apparent rate enhancements are even more remarkable when light scattering in the heterogeneous zeolite medium, which certainly decreases the number of absorbed photons, is taken into account. This movement of the cation also nicely accounts for the observed side selectivity observed in the intrazeolite photo-oxygenation of **15** since movement to the least-substituted side is energetically preferred to give perepoxide **A** rather than **B** (Fig. 6). In fact, calculations by Stratakis and Froudakis (25) have suggested that the cation may already be displaced to the least-substituted side of the alkene before the approach of oxygen. The high barrier for inversion of a heteroatom in three-membered rings dictates that **A** can only collapse by hydrogen abstraction from the least-hindered side of the alkene.

The model shown in Fig. 6 can also explain the end selectivity since the sodium cation acts as an electron sink, withdrawing electron density from the carbon framework. To accommodate the increased amount of positive charge on the carbon framework the C-O bond to the most highly substituted carbon in the perepoxide is lengthened, ultimately resulting in cleavage of that bond and hydrogen abstraction from the most-substituted end of the alkene.

The hydrogen bond steering effect and the stereochemical preference during the intrazeolite photo-oxygenation of **6** is significantly diminished (see Chart 1). The erosion of the influence of an allylic hydroxyl-bearing chiral center can be understood in terms of a Curtin–Hammett analysis (26) as shown in the model depicted in Fig. 7. In the dynamic environment inside the supercage, complexation of the sodium cation to the alkene can take several structural motifs. (Fig. 7) However, the reaction appears to proceed via complex **B**, despite the fact that it may not be the most stable complexation geometry, because the cation finds itself in the ideal geometry to provide maximal stabilization of the transition state (**E** in Fig. 7) for product formation. We cannot unambiguously rule out reaction via transition state F. However, this transition state does not provide a convenient explanation for the increased amount of hydrogen abstraction from the least-substituted side of the alkene (see reaction of **15** in Chart 1). In addition, we point out that even if the equilibrium constant [B]/[C] is 1000, a one-to-one ratio of products can still be achieved if the rate constant for the formation of **E** is 10^3 times larger than the rate constant for formation of F (26). On the other hand, we believe that intramolecular hydrogen bonding (transition state **D** in Fig. 7) cannot compete with the electrostatic interaction of the pendant oxygen with the sodium cation in either perepoxide-like transition state E or F to lower the barrier for product formation. Unfortunately, at the present time we only have relative product ratios inside and outside the zeolite to infer information about the dynamic binding events inside the zeolite supercage. Consequently, we prefer to refer to the suggestion in Fig. 7 as a model rather than a mechanism.

The inability to trap an intrazeolite perepoxide intermediate (Fig. 4) mirrors failed attempts in solution (E. L. Clennan, unpublished). Recently, Singleton and coworkers (27,28) have suggest that the singlet oxygen ene reaction proceeds via two transition states without an intervening intermediate. This topographical arrangement is made possible because these two maxima on the reaction pathway are saddle points on a three-dimensional surface. The first transition state does not involve hydrogen abstraction by the trailing oxygen but leads to the second perepoxide-like transition state. This transition state lies near a valley-ridge inflection where bifurcation to the isomeric allylic hydroperoxides occurs. Consequently, dynamic effects (*i.e.* the momentum of atoms) dictate the product ratio (29). The unsuccessful trapping, although consistent with the Singleton suggestion, is unfortunately a negative result and does not provide evidence, either for or against, intrazeolite electrostatic stabilization of a perepoxide intermediate.

CONCLUSION

Several studies have now confirmed that electrostatic stabilization of a perepoxide or perepoxide-like transition state plays a key role in dictating the regio- and stereochemistry of the intrazeolite singlet oxygen ene reaction (4,30–38). This stabilization leads to operational (apparent) dramatic intrazeolite rate enhancements and can significantly modify or completely replace other noncovalent interactions such as hydrogen bonding, which are important in the homogeneous variant of the singlet oxygen ene reaction. The reactions of these allylic alcohols demonstrate that intrazeolite photo-oxygenations do not always provide an advantage in terms

of either regio- or stereochemical control. However, the use of models such as that shown in Figs. 6 and 7 provide a powerful tool to assess the advantages or disadvantages of using the zeolite environment with a wide range of alkene substrates.

Acknowledgement—We thank the National Science Foundation for their generous support of this research.

REFERENCES

1. Schenck, G. O. (1948) Photosensitized reactions with molecular oxygen. *Naturwissenschaften* **35**, 28–29.
2. Clennan, E. L. (2005) Photo-oxygenation of the ene-type. In *Molecular and Supramolecular Photochemistry,* Vol. 12 (Edited by A. G. Griesbeck and J. Mattay), pp. 365–390. Marcel Dekker, New York.
3. Clennan, E. L. (2000) New mechanistic and synthetic aspects of singlet oxygen chemistry. *Tetrahedron* **56**, 9151–9179.
4. Stratakis, M. and M. Orfanopoulos (2000) Regioselectivity in the ene reaction of singlet oxygen with alkenes. *Tetrahedron* **56**, 1595–1615.
5. Clennan, E. L. and A. Pace (2005) Advances in singlet oxygen chemistry. *Tetrahedron* **61**, 6665–6691.
6. Derouane, E. G., F. Lemos, C. Naccache and F. R. Ribeiro (1992) *Zeolite Microporous Solids: Synthesis, Structure, and Reactivity.* Kluwer Academic Publishers, Dordrecht, The Netherlands.
7. Dyer, A. (1988) *An Introduction to Zeolite Molecular Sieves.* John Wiley & Sons, New York.
8. Li, X. and V. Ramamurthy (1996) Selective oxidation of olefins within organic dye cation-exchanged zeolites. *J. Am. Chem. Soc.* **118**, 10666–10667.
9. Adam, W. and B. Nestler (1993) Hydroxy-directed regio- and diastereoselective ene reaction of singlet oxygen with chiral allylic alcohols. *J. Am. Chem. Soc.* **115**, 5041–5049.
10. Groth, U., M. Jung and T. Vogel (2004) Intramolecular chromium(II)-catalyzed pinacol cross coupling of 2-methylene-α, ω-dicarbonyls. *SynLett* 1054–1058.
11. Hudlicky, T., C. H. Boros and E. E. Boros (1992) A model study directed towards a practical enantioselective total synthesis of (-)-morphine. *Synthesis* 174–178.
12. Yates, P. and G. E. Langford (1981) Synthesis of some bicyclo [2.2.2]oct-5-en-2-ones and bicyclo[2.2.2]octan-2-ones. Rearrangments accompanying oxidative decarboxylation with lead tetraacetate. *Can. J. Chem.* **59**, 344–355.
13. Griesbeck, A. G., W. Adam, A. Bartoschek and T. T. El-Idreesy (2003) Photooxygenation of allylic alcohols: Kinetic comparison of unfunctionalized alkenes with prenol-type allylic alcohols, ethers and acetates. *Photochem. Photobiol. Sci.* **2**, 877–881.
14. House, H. O. (1972) *Modern Synthetic Reactions,* 2nd ed. W. A. Benjamin, Menlo Park, CA.
15. Adam, W., O. Gevert and P. Klug (1994) Photooxygenation of γ-hydroxy vinylstannanes and their acyl derivatives: Mechanistic insight into the hydroxy-directing effects. *Tetrahedron Lett.* **35**, 1681–1684.
16. Adam, W. and B. Nestler (1992) Photooxygenation of chiral allylic alcohols: Hydroxy-directed regio- and diastereoselective ene reaction of singlet oxygen. *J. Am. Chem. Soc.* **114**, 6549–6550.
17. Adam, W. and B. Nestler (1993) (Z)-3-Methyl-3-penten-2-ol as stereochemical probe for 1,2 versus 1,3 allylic strain in the photooxygenation and epoxidation of chiral allylic alcohols. *Tetrahedron Lett.* **34**, 611–614.
18. Adam, W., C. R. Saha-Möller, S. B. Schambony, K. S. Schmid and T. Wirth (1999) Stereocontrolled photooxygenations—A valuable synthetic tool. *Photochem. Photobiol.* **70**, 476–483.
19. Adam, W. and T. Wirth (1999) Hydroxy group directivity in the epoxidation of chiral allylic alcohols: Control of diastereoselectivity through allylic strain and hydrogen bonding. *Acc. Chem. Res.* **32**, 703–710.
20. Prein, M. and W. Adam (1996) The Schenck ene reaction: Diastereoselective oxyfunctionalization with singlet oxygen in synthetic applications. *Angew. Chem. Int. Ed. Engl.* **35**, 477–494.
21. Clennan, E. L. and G. L. Pan (2003) Zeolite-promoted oxidations of 1,1-diarylethylenes. *Org. Lett.* **5**, 4979–4982.
22. Clennan, E. L. (2003) Molecular oxygenations in zeolites. In *Photochemistry of Organic Molecules in Isotropic and Anisotropic Media,* Vol. 9 (Edited by V. Ramamurthy and K. S. Schanze), pp. 275–308. Marcel Dekker, New York.
23. Barich, D. H., T. Xu, J. Zhang and J. F. Haw (1998) Modeling of benzene adsorption in metal exchanged zeolites by calculation of ^{7}Li chemical shifts. *Angew. Chem. Int. Ed. Engl.* **37**, 2530–2531.
24. Ma, J. C. and D. A. Dougherty (1997) The cation-π interaction. *Chem. Rev.* **97**, 1303–1324.
25. Stratakis, M. and G. Froudakis (2000) Site specificity in the photooxidation of some trisubstituted alkenes in thionin-supported zeolite Na-Y. On the role of the alkali metal cation. *Org. Lett.* **2**, 1369–1372.
26. Carey, F. A. and R. J. Sundberg (2000) *Advanced Organic Chemistry. Part A: Structure and Mechanisms.* Kluwer Academic/Plenum Publishers, New York.
27. Singleton, D. A., C. Hang, M. J. Szymanski and E. E. Greenwald (2003) A new form of kinetic isotope effect. Dynamic effects on isotopic selectivity and regiochemistry. *J. Am. Chem. Soc.* **125**, 1176–1177.
28. Singleton, D. A., C. Hang, M. J. Szymanski, M. P. Meyer, A. G. Leach, K. T. Kuwata, J. S. Chen, A. Greer, C. S. Foote and K. N. Houk (2003) Mechanism of ene reactions of singlet oxygen. A two-step no-intermediate mechanism. *J. Am. Chem. Soc.* **125**, 1319–1328.
29. Gonzalez-Lafont, A., M. Moreno and J. M. Lluch (2004) Variational transition state theory as a tool to determine kinetic selectivity in reactions involving a valley-ridge inflection point. *J. Am. Chem. Soc.* **126**, 13089–13094.
30. Clennan, E. L. and J. P. Sram (1999) Photooxidation in zeolites. Part 2: A new mechanistic model for reaction selectivity in singlet oxygen ene reactions in zeolitic media. *Tetrahedron Lett.* **40**, 5275–5278.
31. Clennan, E. L. and J. P. Sram (2000) Photochemical reactions in the interior of a zeolite. Part 5. The origin of the zeolite induced regioselectivity in the singlet oxygen ene reaction. *Tetrahedron* **56**, 6945–6950.
32. Clennan, E. L., J. P. Sram, A. Pace, K. Vincer and S. White (2002) Intrazeolite photooxidations of electron-poor alkenes. *J. Org. Chem.* **67**, 3975–3978.
33. Shailaja, J., J. Sivaguru, R. J. Robbins, V. Ramamurthy, R. B. Sunoj and J. Chandrasekhar (2000) Singlet oxygen mediated oxidation of olefins within zeolites: Selectivity and complexities. *Tetrahedron* **56**, 6927–6943.
34. Stratakis, M., D. Kalaitzakis, D. Stavroulakis, G. Kosmas and C. Tsangarakis (2003) Remarkable change of the diastereoselection in the dye-sensitized ene hydroperoxidation of chiral alkenes by zeolite confinement. *Org. Lett.* **5**, 3471–3474.
35. Stratakis, M. and G. Kosmas (2001) Enhanced diastereoselectivity of an ene hydroperoxidation reaction by confinement within zeolite Na-Y; a stereoisotopic study. *Tetrahedron Lett.* **42**, 6007–6009.
36. Stratakis, M., R. Nencka, C. Rabalakos, W. Adam and O. Krebs (2002) Thionin-sensitized intrazeolite photooxygenation of trisubstituted alkenes: Substituent effects on the regioselectivity as probed through isotopic labeling. *J. Org. Chem.* **67**, 8758–8763.
37. Stratakis, M., C. Rabalakos, G. Mpourmpakis and G. E. Froudakis (2003) Ene hydroperoxidation of isobutenylarenes within dye-exchanged zeolite Na-Y: Control of site selectivity by cation-arene interactions. *J. Org. Chem.* **68**, 2839–2843.
38. Stratakis, M. and N. Sofikiti (2002) Intrazeolite photo-oxygenation of (R)-(-)-alpha-phellandrene. *J. Chem. Res.* **-S**, 374–375.